Biomaterials 258 (2020) 120310

Contents lists available at ScienceDirect

Biomaterials

journal homepage: www.elsevier.com/locate/biomaterials

Leading Opinion

Autologous cell membrane coatings on tissue engineering xenografts for suppression and alleviation of acute host immune responses

Chao Tao [a,b], Xiaolei Nie [a], Wenzhen Zhu [a], Jabed Iqbal [c], Chenjie Xu [a], Dong-An Wang [b,*]

[a] School of Chemical and Biomedical Engineering, Nanyang Technological University, 50 Nanyang Ave, 639798, Singapore
[b] Department of Biomedical Engineering, City University of Hong Kong, Tat Chee Avenue, Kowloon, Hong Kong
[c] Department of Pathology, Singapore General Hospital, 20 College Road, Academia, Diagnostics Tower, Level 10, 169856, Singapore

ARTICLE INFO

Keywords:
Cell membrane
Coating
Immunocompatibility
Tissue engineering
Extracellular matrix
Xenograft

ABSTRACT

Xenogeneic extracellular matrix (ECM) based tissue engineering graft is one of the most promising products for transplantation therapies, which could alleviate the pain of patients and reduce surgery cost. However, in order to put ECM based xenografts into clinical use, the induced inflammatory and immune responses have yet to be resolved. Cell membrane is embedded with membrane proteins for regulation of cell interactions including self-recognition and potent in reducing foreign body rejections. In this study, a novel and facile method for evasion from immune system was developed by coating autologous red blood cell membrane as a disguise on xenogeneic ECM based tissue engineering graft surface. Porcine source Living Hyaline Cartilage Graft (LhCG) and decellularized LhCG (dLhCG) established by our group for cartilage tissue engineering were chosen as model grafts. The cell membrane coating was quite stable on xenografts with no obvious decrease in amount for 4 weeks. The autologous cell membrane coated xenograft has been proved to be recognized as "self" by immune system on cell, protein and gene levels according to the 14-day lasting *in vivo* study on rats with less inflammatory cells infiltrated and low inflammation-related cytokines gene expression, showing alleviated acute immune and inflammatory responses.

1. Introduction

Implants for tissue engineering could be categorized into xenografts, derived from heterologous animals, allografts, derived from another individual of the same species with a different genotype, autografts, derived from the same individual, and synthetic biomaterials, according to the source. It is worth noting that not eliciting severe immune and inflammatory responses is a key for long-term survival of the implants [1]. Besides, autografts are believed to be less likely to induce immune and inflammatory responses than allografts and xenografts [2,3].

Approaches based on natural extracellular matrix (ECM) have attracted more and more attention for tissue engineering [4–6]. ECM is the 3D microenvironment of resident cells in tissue, consisting of cell secreting structural and functional molecules [7,8]. It's reported that ECM based implants have been successfully used in regeneration of heart valves [9], abdominal walls [10] and even commercially used (*eg.* AlloDerm®, Oasis®) [11]. The cell-derived ECM is superior to synthetic biomaterials derived hydrogels to better mimic the healthy situation so that the cells are more willing to attach and proliferate on the lesion site [7]. Moreover, degradation rate of synthetic biomaterials scaffolds is difficult to control. Scaffold residues will interfere cell-cell signaling and further tissue growth or morphogenesis [11]. In this case, the scaffold-free neotissue based on ECM is a promising biocompatible implant for tissue engineering [6,10,11]. For example, an autologous ECM graft was engineered by culturing autologous cells in a 3D poly (lactide-*co*-glycolide) (PLGA) template, subsequent decellularization and removal of template [12]. And further 3D stepwise chondrogenesis-mimicking ECM graft by controlling the stages of chondrogenic differentiation was studied [13].

However, in order to address the problem of limited autografts and allografts source, reduce surgery cost and relieve the pain of patients [14], more and more researchers have been focusing on xenografts such as implants based on ECMs secreted by *in vitro* cultured porcine or bovine cells [4,15]. Our group has been studying cartilage tissue engineering based on porcine source ECM for years and established Living Hyaline Cartilage Graft (LhCG) system for tissue regeneration [16–19]. Decellularized LhCG (dLhCG) was further developed and studied [20–22]. It is inevitable that xenografts accompany with concerns of

* Corresponding author.
E-mail address: dwang229@cityu.edu.hk (D.-A. Wang).

https://doi.org/10.1016/j.biomaterials.2020.120310
Received 6 March 2020; Received in revised form 13 July 2020; Accepted 7 August 2020
Available online 11 August 2020
0142-9612/© 2020 Elsevier Ltd. All rights reserved.

their biocompatibility [23], which threatens long term survival of the implants and even the life of patients. For example, the proteoglycans and collagens of xenogeneic derived ECM have antigenic properties that will elicit immune responses in the host due to different sequences of homologous proteins between human and heterogeneous animals such as pig [24–26]. In addition, anti-non-gal antibodies in human will bind with and further degrade xenogeneic ECM implants by recruiting macrophages and inducing proteolytic activity of macrophages [27]. Moreover, cell residues caused by incomplete decellularization could further initiate immune rejection. As a result, although tissue engineering implant based on xenogeneic decellularized ECM is promising, immune rejection by the host needs to be addressed for clinical use. More and more researchers have been focusing on investigating and enhancing the immunocompatibility of xenografts [28–35], such as using genetically engineered pigs [36]. However, current methods for alleviating immune responses of xenografts including antigen removal [37], glutaraldehyde crosslinking [27] and treatment post-surgery [38] would result in tedious fabrication process, sacrifice of regeneration effect or suffer in patients. In this case, simplified and efficient new methods to suppress or alleviate inflammatory and immune responses of xenografts are needed. Coating natural biological materials such as cell membrane is simple and safe with moderate operation environment and at the same time reserves nature of biological materials [39,40].

As for other fields such as drug delivery and biomedical devices, biocompatibility including immunocompatibility has also attracted much attention [41–43]. Cell membrane coated nanoparticles have been widely applied in drug delivery for evasion from immune system [44,45]. Cell membrane is a phospholipid bilayer embedded with biomacromolecules such as sugars and proteins which govern cell functions including interactions with biological materials or biomaterials. Therefore, the biological functions could be transferred and performed by coating cell membrane onto biomaterials. Cell membrane-derived materials have been utilized to increase biocompatibility [46]. CD47 is a "marker of self" glycoprotein which is expressed on cell membranes of all mammals. CD47 could interact with CD172a, also known as signal regulatory protein-α (SIRPα), on macrophages to inhibit phagocytes [47]. Furthermore, it is reported other membrane proteins on RBC membrane such as complement receptor 1 and membrane cofactor protein could defense against attack from complement system [48]. Nowadays, cell membrane coated nanoparticles have been widely studied for drug delivery and shown potential in immune evasion [48–50]. In addition, cell membrane coating has been successfully applied onto nanomotors [51] and nanofiber scaffold [52]. We herein considered applying autologous cell membrane coating on xenografts, taking advantage of its embedded protein in cell membrane which contributes to the disguise of xenografts and recognition as self by the host.

In this study, a facile method was developed by coating autologous cell membrane onto xenografts to attenuate the immune and inflammatory responses (Fig. 1). Red blood cell (RBC), due to its abundance in human bodies and accessibility, is believed to be an appropriate choice for the autologous cell membrane source. The basic idea for clinical use is collecting blood from the patients before surgery, after which the RBCs are separated and lysed for cell membrane which are further coated onto xenografts for implantation. LhCG, which contains mainly porcine chondrocytes and ECM, and dLhCG, which is mainly composed by porcine derived ECM, established by our group for cartilage tissue engineering were chosen as model xenografts and coated with autologous RBC membrane as a disguise from immune system, so that the xenografts could be recognized as autografts. This approach potentially contributed to survival and further clinical translation of xenogeneic ECM based grafts.

2. Materials and methods

2.1. Materials

3,3′-dioctadecylox-acarbocyanine perchlorate (DiO) was purchased from Sigma Aldrich and dissolved in dimethyl sulfoxide (DMSO) (Sigma Aldrich, USA) before use. Porcine chondrocytes for LhCG and dLhCG fabrication were extracted from commercially available porcine bone from market. Whole blood for RBC membrane extraction was collected from rat's tails.

2.2. Derivation and characterization of cell membrane vesicles and coating

RBC membrane vesicles were prepared according to a published protocol [44]. Briefly, whole blood was centrifuged at 800×*g* at 4 °C for 5min, after which the serum and fluffy precipitation on the surface were carefully removed. The collected RBCs were washed with cold 1 × phosphate buffered saline (PBS, Gibco, USA) for three times. Then the RBCs were suspended in 10 mmol/L Tris-HCl buffer (pH = 7.4, 1st Base Pte Ltd, Singapore) at 4 °C for 1 h for hemolysis treatment. The white pellet (RBC membrane) was collected after centrifuge at 800×*g* for 5min and washed with the hypotonic buffer. The finally collected RBC membrane was sonicated for 5min with a sonicator (XUB5, Chemosclence Pte Ltd, Singapore) at 60 Hz and 250 W to promote the self-assembly of cell membrane before coating.

Dynamic light scattering (DLS) was performed on a Malvern Nano-ZS for measurement of RBC membrane vesicles' size and zeta potential. Samples were prepared by suspending cell membrane vesicles with deionized (DI) water.

RBC membrane vesicles were suspended and diluted in DI water and spread on a slide of silicon wafer. The samples were dried at room temperature and scanned by atomic force microscopy (AFM) (CSPM5500A, Being NanoInstruments Ltd., China).

Attenuated total reflectance-fourier transform infrared reflection (ATR-FTIR) (Smart iTR, Thermo Fisher Scientific Inc., Singapore) was carried out for determination of chemical structure of cell membrane

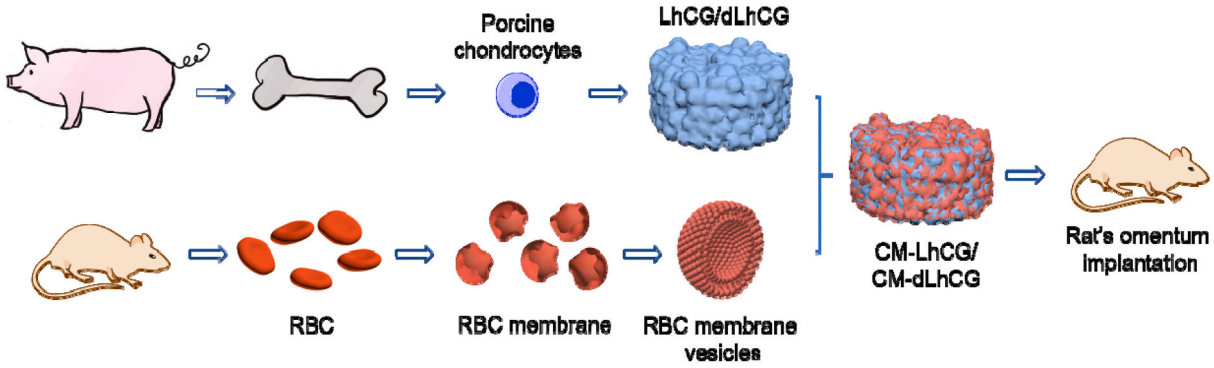

Fig. 1. Schematic illustration of the design of RBC membrane coated xenografts.

components. Cell membrane sample was freeze-dried for ATR-FTIR measurement.

For verification of the feasibility of coating formation, cell membrane suspended in DI water was coated onto silicon (Si) (SUNSON, China), coverslip (CellPath Ltd, UK) and natural porcine cartilage surfaces by drip coating then drying overnight at room temperature. Water contact angle was conducted on a Kruss DSA25 Contact Angle Analyzer with a 5 μL DI water drop. Five samples were measured and averaged for the final water contact angle value.

2.3. Cell membrane coating on grafts

LhCG and dLhCG were engineered based on an established protocol in our previous publications as model xenografts [16–19]. dLhCG is a promising candidate for cartilage tissue engineering [20–22]. LhCG was also chosen as a control as well as a template for illustration of the RBC membrane effect. Briefly, porcine hyaline chondrocytes were extracted from porcine cartilage and encapsulated with gelatin (gelatin from bovine skin, Sigma Aldrich, USA) microspheres in alginate (Alginic acid sodium salt, Sigma Aldrich, USA). The cells outgrew and filled up the cavities, forming pure micro-tissues. After the 3D ECM was secreted and stable, the alginate hydrogel was removed by sodium citrate (Sigma Aldrich, USA) solution (55 mM in 0.15 M NaCl) for a cartilaginous ECM and chondrocyte-based graft LhCG. LhCG was decellularized by sequential physical, chemical and enzymatic treatments to harvest dLhCG.

LhCG and dLhCG samples were rinsed in RBC membrane vesicles which were suspended in Dulbecco's Modified Eagle's Medium (DMEM) or 1 × PBS, respectively for 1 h for coating, followed by rinse in pure culture medium or DI water respectively for 30min to wash the uncoated cell membrane. 0.6 mL whole blood was used to extract cell membrane components to coat LhCG and dLhCG which were around 0.5 cm in diameter. Finally, we got the cell membrane coated LhCG (CM-LhCG) and cell membrane coated dLhCG (CM-dLhCG).

2.4. Visualization and detection of cell membrane coating on grafts

For visualization of cell membrane coatings on LhCG and dLhCG, DiO, a lipophilic tracer, was used to label cell membrane and observed under a fluorescent microscope (Olympus IX71S1F-3, Japan). The dyed samples were embedded in paraffin (Surgipath® Paraplast®, Leica, USA) and sectioned on a slicer (RM2255, Leica, USA) before observation.

X-ray photoelectron spectroscopy (XPS) was operated on a Kratos AXIS Supra spectrometer with a bandpass energy of 40eV to detect carbon (C), oxygen (O), nitrogen (N), phosphorous (P) and sulfur (S). The high-resolution spectrum of C was fitted by Origin 9.0 software. dLhCG and CM-dLhCG samples were freeze-dried (BT48, Millrock Technology Inc, USA), while LhCG and CM-LhCG samples were fixed in 2.5v/v% glutaraldehyde (Sigma Aldrich, USA), dehydrated in gradient ethanol, followed by dried in a critical point dryer (K850, Quorum Technologies Inc., England).

2.5. Stability of cell membrane coatings

dLhCG is decellularized ECM consisting of glycosaminoglycan and glycoproteins. Cell membrane is a phospholipid embedded with membrane proteins. Therefore, almost all phosphorus comes from cell membrane components. In this case, the phosphorus content could reflect the cell membrane content on the surface. Phosphorus of CM-dLhCG samples was measured by inductively coupled plasma mass spectrometry (ICP-MS) (Elan-DRCe, PerkinElmer SCIEX, USA) as quantification of cell membrane coatings. First, CM-dLhCG was digested by papain (1 mg/mL in DI water, Sigma Aldrich, USA) at 60 °C overnight. Then the solution was diluted 50 times in DI water with 1% HCl. CM-dLhCG samples, which were rinsed in DI water for 1 d, 7 d, 14 d and 28 d, were measured to investigate the stability of the cell membrane coatings. DI water was chosen as the medium to avoid the interference of possible P content in the solution. P content of dLhCG was also measured.

For LhCG samples, RBC membrane dyed with DiO beforehand during the extraction process (CM-DiO) was coated onto LhCG and fixed in 4% paraformaldehyde on 1 d, 7 d, 14 d and 28 d, respectively. The fixed samples were further embedded in paraffin, sectioned into 10 μm thick and observed under fluorescent microscope.

2.6. Morphology of grafts

The morphology of LhCG, CM-LhCG, dLhCG and CM-dLhCG was observed under scanning electronic microscopy (SEM) (JEOL JSM 6700F, Japan). dLhCG and CM-dLhCG samples were freeze-dried, while LhCG and CM-LhCG samples were fixed in 2.5v/v% glutaraldehyde, dehydrated in gradient ethanol, followed by dried in a critical point dryer. All samples were coated with platinum by sputtering for 120s (JFC-1600, JEOL Asia Pte. Ltd., Japan) before SEM observation.

2.7. In vivo rat omentum implantation model

All animal experiment protocols have been approved by Institutional Animal Care and Use Committee (IACUC), Singapore according to the local law.

The *in vivo* studies on immune and inflammatory responses were performed on sixty-four Sprague Dawley female rats (n = 4, 250–300 g) by an omentum implantation model. Omentum was chosen due to its sensitivity to foreign bodies. If the grafts could survive in omentum, it will be more convincing for the grafts not to elicit immune responses in other organs or tissues, especially the immune privileged sites such as skin and cartilage. All the rats were randomly divided into eight groups. Two groups of rats were implanted with dLhCG (Xeno-d) and LhCG (Xeno), respectively. Rats implanted with CM-dLhCG of which RBC collected from other or the same rats were labeled as Allo-d and Auto-d, respectively. Similarly, rats implanted with CM-LhCG of which RBC collected from other or the same rats were labeled as Allo and Auto, respectively. Then the grafts (~0.5 cm in diameter) were washed with sterile PBS before embedded into rats' omentum. Before surgery, blood was collected from tails of rats and coated onto dLhCG and LhCG for the fabrication of CM-dLhCG and CM-LhCG samples. 0.6 mL whole blood was used for harvest of cell membrane coating for one graft with size of around 0.5 cm in diameter. During the surgery, an approx. 2 cm incision was firstly made on the rats' abdomen. Two grafts of the same group were then embedded into each rat before closure of the incision with 4-0 Nylon sutures and stainless-steel clips. On post-surgical day 1 and day 14, after sacrifice of the animals, the two implanted grafts in each rat, as well as the surrounding tissues were collected from the surgical sites, and kept in 4% paraformaldehyde (Sigma Aldrich, USA) or 1 × PBS respectively for the following experiments. Samples collected on day 1 were labeled as Xeno1, Xeno-d1, Allo1, Allo-d1, Auto1 and Auto-d1, respectively. Similarly, samples collected on day 14 were labeled as Xeno14, Xeno-d14, Allo14, Allo-d14, Auto14 and Auto-d14, respectively. Natural xenogeneic cartilage slices with 0.5 cm in diameter were punched from porcine articular cartilage, decellularized, embedded into rats and collected on day 1 (PC1) and day 14 (PC14) post-operation according to the same protocol mentioned above as a positive control. Natural autologous cartilage with 0.5 cm in diameter was punched from rat ear, embedded into the same individual and collected on day 1 (RE1) and day 14 (RE14) post-operation according to the same protocol mentioned above as a negative control.

2.8. Histological and immunohistochemical analysis

The collected samples fixed in 4% paraformaldehyde were embedded in paraffin and sectioned into 10 μm thick on a slicer

(RM2255, Leica, USA). The sectioned samples were deparaffined and rehydrated before staining.

Hematoxylin and Eosin (H&E) staining (Sigma Aldrich, USA) was carried out according to a standard protocol of the manufacturer. Immune and inflammatory responses on cell level were evaluated based on numbers of inflammatory cells by scoring [35,37,53,54] according to a five-point grading scheme by a pathologist who was blinded to experiment design and groups.

Immunohistochemistry (IHC) staining of MPO, CD68 and CD3 was performed with UltraVision™ Quanto Detection System HRP DAB kit (Thermo Fisher Scientific, UK) based on the standard protocol of the manufacturer for detection of neutrophils, macrophages and T cells, respectively. The details of antibodies were listed in Supplemental Table 1. The slides were finally mounted with Surgipath® Micromount (LeicaBiosystems, USA).

2.9. Gene expression

Quantitative real-time polymerase chain reaction (qRT-PCR) was conducted to evaluate inflammatory responses on a gene level by detecting gene expression of inflammation-related cytokines. The target gene expression was also confirmed by agarose gel electrophoresis.

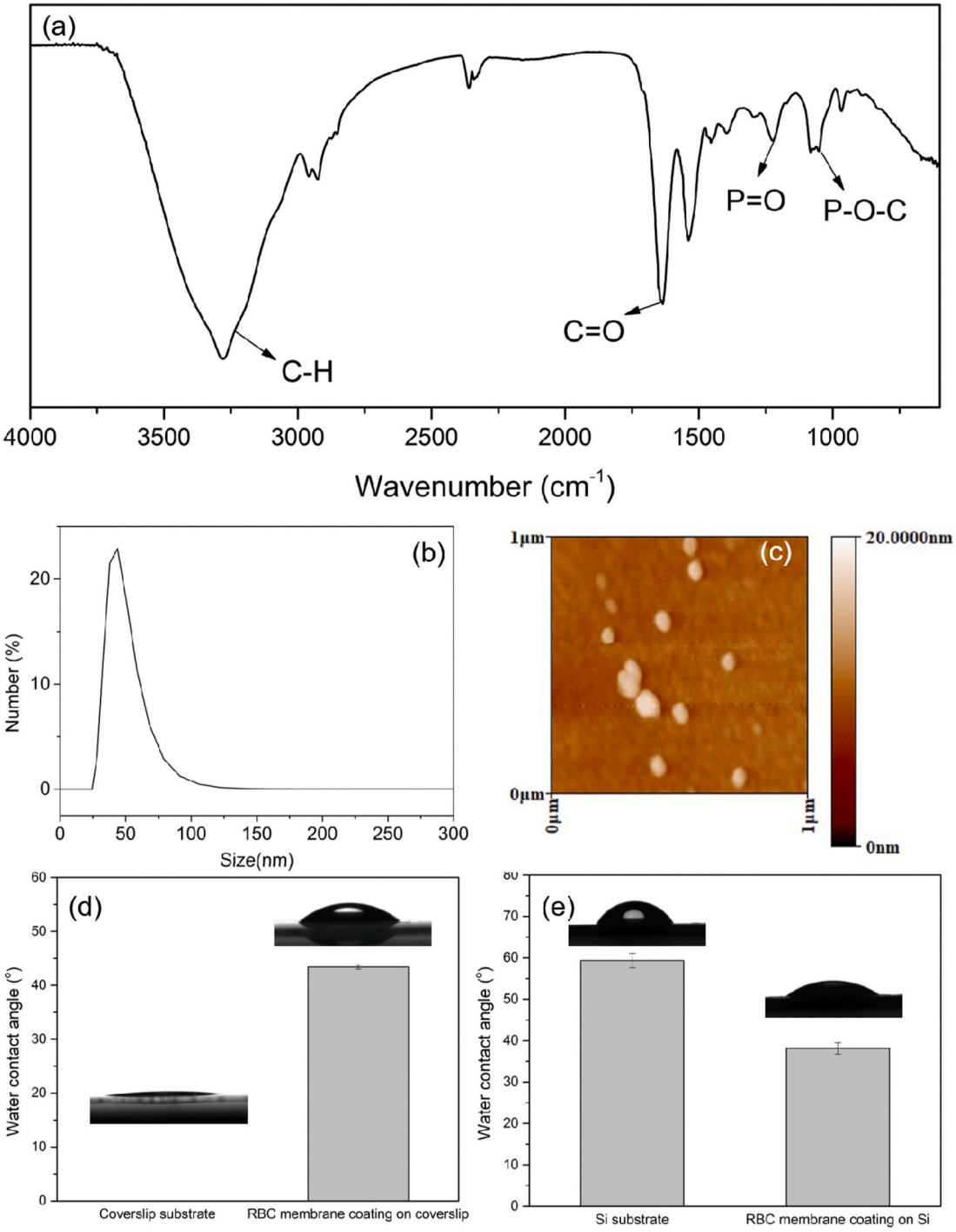

Fig. 2. (a) ATR-FTIR spectrum of RBC membrane, (b) DLS result and (c) AFM image of RBC membrane vesicles, water contact angle of (d) coverslip and (e) Si surfaces respectively with and without RBC membrane coating.

Total RNA of the graft with surrounding tissues was isolated by TRIzol® reagent (Life Technology, USA) from samples kept in 1 × PBS according to the manufacture's protocol and the RNA concentration was tested by NanoDrop 2000c (ThermoFisher Scientific, USA). Then total RNA was reverse transcribed to cDNA. A 12 μL reaction volume containing 500 ng of RNA, 1 μL Oligo dT was used for first-strand cDNA synthesis reaction. The mixture was heated to 70 °C for 5min and quickly cooled on ice for 15min. Afterwards, 5 × reaction buffer (5 μL), dNTP Mix (1.25 μL, 10 mM), M-MLV RT RNase (H-) Pt Mutant (0.5 μL) and DI water were added. All the reverse transcription reagents were purchased from Promega, USA. The reaction mixture was incubated at 40 °C for 10min, 50 °C for 50min and then 70 °C for 15min, after which the first-strand cDNA was generated.

qRT-PCR was conducted by SYBR Green chemistry on a CFX Connect Real-Time PCR System (BIO-RAD, USA) with a 20 μL reaction mixture containing 1 μL cDNA, 1.2 μL primers, 10 μL SsoAdvanced™ Universal SYBR® Green Supermix (BIO-RAD, USA) and DI water. The primers used for qRT-PCR were purchased from Integrated DNA Technologies, Singapore and listed in Supplemental Table 2. The qRT-PCR results of target genes were normalized against a housekeeping gene (*GAPDH* gene) and calculated by the comparative $2^{-\Delta\Delta C}{}_{T}$ method.

On the other hand, cDNA was amplified using Taq DNA polymerase (NEW ENGLAND BioLabs, England) for semi-quantitative PCR. Thermal cycle was performed as follows: 95 °C for 30s followed by 30 cycles of 95 °C for 30s, annealing at 55 °C for 30s, 68 °C for 30s, and a final extension at 68 °C for 5min. The products were visualized on 1.5% agarose gels in Tris-Borate-EDTA Buffer (Vivantis Technologies, Malaysia) with SYBR® Safe DNA gel stain (Invitrogen, USA).

3. Results

3.1. Derivation of cell membrane vesicles and coatings

First of all, cell membrane was extracted and cell membrane vesicles were characterized by DLS and AFM. The chemical structure of the extracted cell membrane was confirmed by ATR-FTIR.

As is shown in ATR-FTIR spectrum of RBC membrane (Fig. 2a), peaks at 3282 cm^{-1} and 1635 cm^{-1} belong to C–H stretching vibration and C═O stretching vibration, respectively. The peaks of P═O stretching vibration (1224 cm^{-1}) and P–O–C stretching vibration (1081 cm^{-1}) belong to the hydrophilic phosphate head of phospholipids and confirm the successful extraction of cell membrane.

According to DLS results, the cell membrane vesicles were 52.32 ± 3.77 nm in size with a PDI of 0.61 ± 0.04 (Fig. 2b), which is in consistent with the AFM results (Fig. 2c). And the zeta potential was −28.97 ± 0.82 mV, in accordance with the literature [55].

In order to confirm the feasibility of cell membrane coating formation, RBC membrane was firstly coated onto coverslip, Si and natural porcine cartilage surfaces, respectively. Water contact angles were measured and shown in Fig. 2d and e as well as Figure S1. Coverslip has a superhydrophilic surface whose water contact angle is below 5°. Water contact angle of coverslip increased to 43.4°±0.4° with RBC membrane coating on the surface (Fig. 2d). In addition, Si surface became more hydrophilic with water contact angle decreasing to 38.1°±1.4° from 59.4°±1.8° after coated with RBC membrane (Fig. 2e). After coated with RBC membrane, cartilage surface's water contact angle decreased from 71.3 ± 1.0° to 37.6 ± 2.0° (Figure S1). The above water contact angle results confirmed successful coating formation on both coverslip and Si surfaces as well as cartilage surfaces which resembled LhCG and dLhCG surfaces, after which RBC membrane was further coated onto dLhCG and LhCG surfaces, respectively.

3.2. Characterization and stability of cell membrane coating on grafts

The visualization and characterization of RBC membrane coating on grafts were achieved by fluorescent microscopy and XPS. DiO, a lipophilic tracer which will emit green fluorescence when conjugated with cell membrane and excited by blue light, was used to label RBC membrane in advance. Fluorescent image (Fig. 3a and b) confirmed the successful coating of cell membrane.

Elemental information on the surface within a depth of 10 nm could be detected by XPS. In order to investigate the difference in surface chemistry among the four kinds of grafts, XPS was carried out (Fig. 4). dLhCG which had been decellularized constituted primarily glycoproteins and glycosaminoglycan (GAG) [16], while cell membrane was mainly made of phospholipids. Therefore, LhCG and CM-LhCG had a relatively higher level of P content, which came from cell membrane, compared to dLhCG and CM-dLhCG (Table 1). As is shown in Fig. 4a, P 2p peak at around 132 eV of dLhCG was almost invisible, indicating an absence of cell membrane in dLhCG. Moreover, P content of dLhCG increased from 0.7% to 2.4% after coated with RBC membrane (Table 1), further showing successful coating of RBC membrane on dLhCG surface. There was also a slight increase in P content of CM-LhCG (3.4%) compared to LhCG (2.9%), indicating successful coating on LhCG. According to our previous studies [21], there is a loss of GAG during decellularization of LhCG, resulting in a decrease of S content in dLhCG (3.3%) compared to that of LhCG (5.4%), which is also reflected in S content in CM-dLhCG (2.5%) and CM-LhCG (4.8%).

Furthermore, the high resolution of C 1s spectra were fitted with peaks at 284.6eV (C–C, C–H), 286.0eV (C–N, C–S, C–O), 287.8eV (C═O) and 288.7eV (-O-C═O) and shown in Fig. 4b–e.

After the graft is implanted into the injured sites, it takes time for the cells to migrate in and grow. So how long cell membrane would stay on the graft, that is, the stability of cell membrane coating is a following issue that should be taken into consideration. For CM-dLhCG samples, ICP-MS was used to detect the P element content to reflect the cell membrane content and stability [56,57]. dLhCG, consisting mainly of glycoproteins and GAG, barely contains phosphorus. However, cell membrane was mainly made of phospholipids. Therefore, almost all phosphorus is supposed to come from cell membrane coatings in CM-dLhCG. In this case, the amount of cell membrane coatings could be reflected by P content detected by ICP-MS, which could be accurate to ppt level. As is shown in Fig. 5a, the cell membrane coating was quite stable and no obvious decrease in P content was observed from 1 d to 28 d. This implied the strong affinity between cell membrane coatings with dLhCG surface and guaranteed the long-term use of graft *in vivo*. This high affinity might also result from the high surface energy of cell membrane vesicles in aqueous environment. The cell membrane vesicles were so unstable that the adherence to graft surface was irreversible. For CM-LhCG, RBC membrane was dyed by DiO beforehand (CM-DiO) during extraction process and detected by fluorescent microscope in order to investigate its stability. According to Fig. 5b–e, RBC membrane was detected coated on the surface of LhCG as well as adhering to some chondrocytes surface on day 1 and day 7. On day 14 and day 28, though the fluorescence was not as obvious, there was still cell membrane coating detected on surface of LhCG.

3.3. Morphology of grafts

SEM was used to detect the morphology of the grafts with and without cell membrane coatings, respectively. As is shown in Fig. 3, the coating of cell membrane did not change morphology or surface roughness, which was in tens of microns, of dLhCG or LhCG. The coating process did not destroy the porous structure of dLhCG. For LhCG (Fig. 3e) and CM-LhCG (Fig. 3f) samples, chondrocytes were observed aggregating under SEM in the dried samples. LhCG and CM-LhCG samples showed a relatively densely packed structure compared to the porous structure of dLhCG (Fig. 3b) and CM-dLhCG (Fig. 3c).

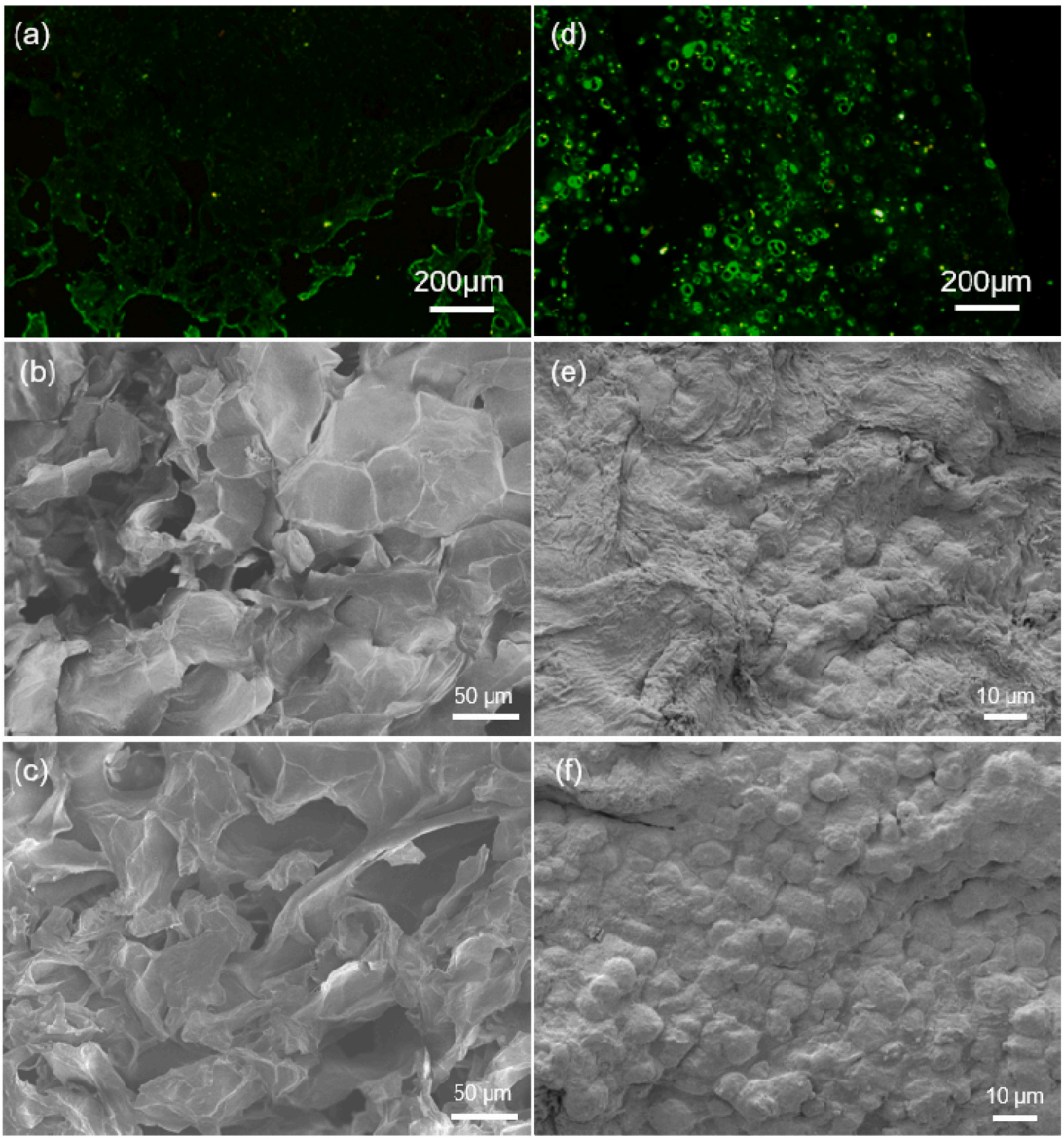

Fig. 3. Fluorescent image of (a) CM-dLhCG and (d) CM-LhCG with DiO-dyed RBC membrane coating and SEM image of (b) dLhCG, (c) CM-dLhCG, (e) LhCG and (f) CM-LhCG.

3.4. In vivo immunocompatibility study by a rat omentum implantation model

The acute inflammatory and immune responses were evaluated on cell, protein and gene levels by pathological analysis, IHC staining and PCR, respectively. Photos of collected grafts from sacrificed rats on day 1 and day 14 post-implantation were shown in Fig. 6a. Xeno, Allo and Auto grafts with relatively densely packed structures which were confirmed in Fig. 3e and f remained original cylinder shape. Xeno-d, Allo-d and Auto-d grafts collected on day 1 became spindle-like. This might be resulted from dehydration of the porous dLhCG grafts *in vivo* as time went by.

3.4.1. Pathological analysis

The quantitative assessment of acute inflammatory and immune responses was determined by a pathologist who was blinded to the design and groups of the experiment according to a five-point grading scheme. White blood cells including neutrophils, macrophages and lymphocytes were evaluated. According to the pathologist, neutrophils have multiple nuclear lobes with usually no granules. Macrophages are recognized as small ovoid or indented nuclei with relatively abundant cytoplasm, while lymphocytes as round dark nuclei with scant cytoplasm. The results and 5-point grading system were listed in Fig. 6b–e.

First of all, all rats survived, indicating there was no hyperacute rejection. On day 1 post-implantation, Allo-d graft showed the most severe neutrophils recruitment followed by Xeno-d graft. By contrast, neutrophils infiltration significantly reduced to minimal in Auto-d graft. There were less neutrophils infiltrated in Auto graft compared to Xeno and Allo grafts which were mild in neutrophils infiltration. For positive control, PC sample showed a mild neutrophils recruitment. For negative control, RE sample induced minimal neutrophils invasion (Fig. 6b). Furthermore, Allo and Allo-d grafts showed the most severe macrophages infiltration followed by Xeno, Xeno-d grafts and PC sample with relatively moderate macrophages infiltration. There were less macrophages present in Auto, Auto-d grafts as well as RE samples. The macrophages infiltration reduced to minimal in Auto-d graft compared to Xeno and Allo grafts. And less macrophages were observed in Auto graft compared Xeno and Allo grafts (Fig. 6c). All groups demonstrated a relatively slighter lymphocytes infiltration with no significant difference between each other. PC sample showed moderate infiltration which was the most severe in all the groups. Xeno, Allo, Xeno-d and Allo-d grafts were mild in lymphocytes invasion, while Auto, Auto-d grafts and RE

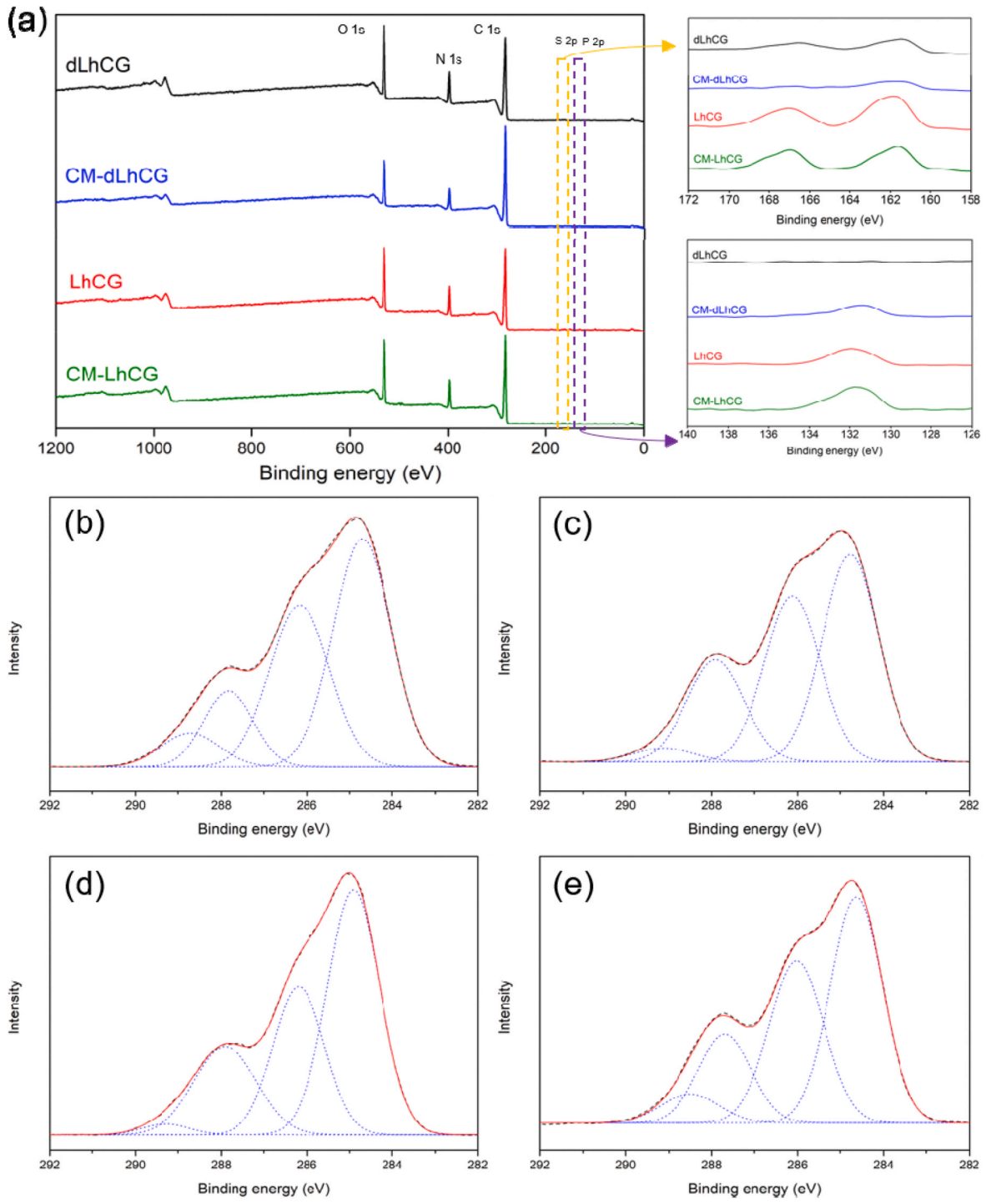

Fig. 4. (a)XPS spectra of dLhCG, CM-dLhCG, LhCG and CM-LhCG, P 2p and S 2p spectra were zoomed in and shown by side, XPS spectrum of C 1s for (b) dLhCG, (c) CM-dLhCG, (d) LhCG and (e) CM-LhCG.

Table 1
Surface elemental composition of dLhCG, CM-dLhCG, LhCG and CM-LhCG.

	C (%)				O (%)	N (%)	P (%)	S (%)
	C–C/C–H	C–N/C–S/C–O	C=O	-O-C=O				
dLhCG	17.8	16.0	4.0	3.9	32.0	22.3	0.7	3.3
CM-dLhCG	29.7	19.9	9.2	0.7	18.3	17.3	2.4	2.5
LhCG	18.0	15.5	5.0	2.8	28.9	21.5	2.9	5.4
CM-LhCG	15.7	17.6	6.4	3.5	28.6	20.0	3.4	4.8

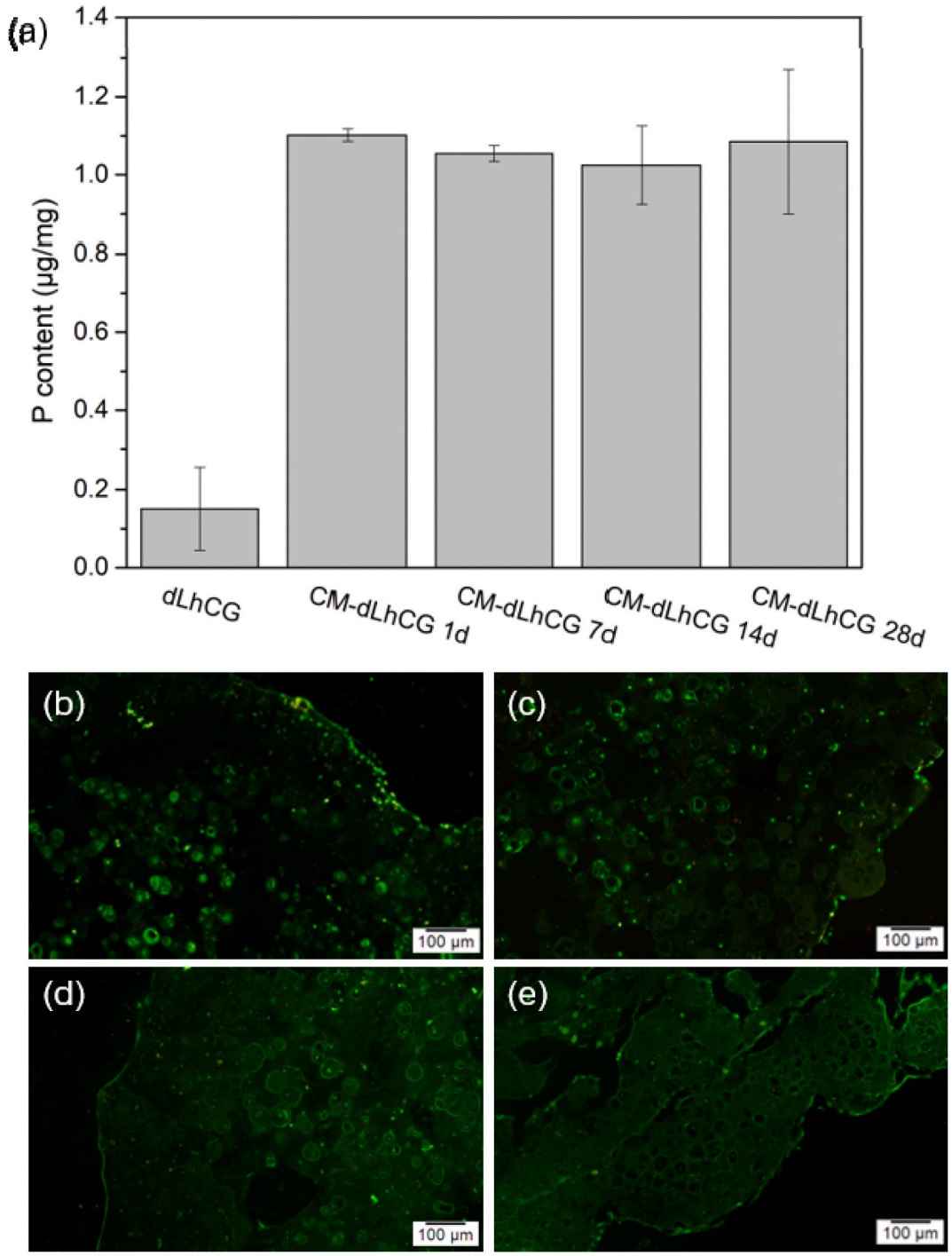

Fig. 5. (a) ICP-MS results of P in CM-dLhCG rinsed in DI water for 1 d, 7 d, 14 d and 28 d, respectively and that of dLhCG; fluorescent image of CM-DiO coated LhCG for (b) 1 d, (c) 7 d, (d) 14 d and (e) 28 d, respectively.

sample showed minimal lymphocytes infiltration (Fig. 6d). On day 14 post-implantation, minimal neutrophils infiltration was observed in all grafts except Auto-d with rare neutrophils detected (Fig. 6b). Macrophages infiltration was even more robust in Allo, Xeno-d and Xeno grafts compared to day 1 results, while it stayed minimal in Auto-d graft and RE sample. Moreover, there were moderate macrophages observed in Allo-d graft and PC sample (Fig. 6c). Lymphocytes infiltration increased to moderate in Allo graft, PC sample and Xeno-d graft on day 14, became slightly worse in Xeno, Allo-d grafts and stayed minimal in Auto, Auto-d grafts and RE sample (Fig. 6d).

3.4.2. Immunohistochemistry staining

Furthermore, immunohistochemistry staining of neutrophils (MPO), macrophages (CD68) and T cells (CD3) was carried out for further study on immune and inflammatory responses on a protein level. H&E and IHC staining results for grafts collected on day 1 and day 14 were listed in Fig. 7, respectively.

IHC staining of neutrophils (MPO), macrophages (CD68) and T cells (CD3) of implanted grafts (Fig. 7) as well as autologous rat ear (Figure S2) and decellularized porcine cartilage (Figure S3) was carried out. H&E staining was carried out for comparison. The IHC staining results were in accordance with the pathological analysis.

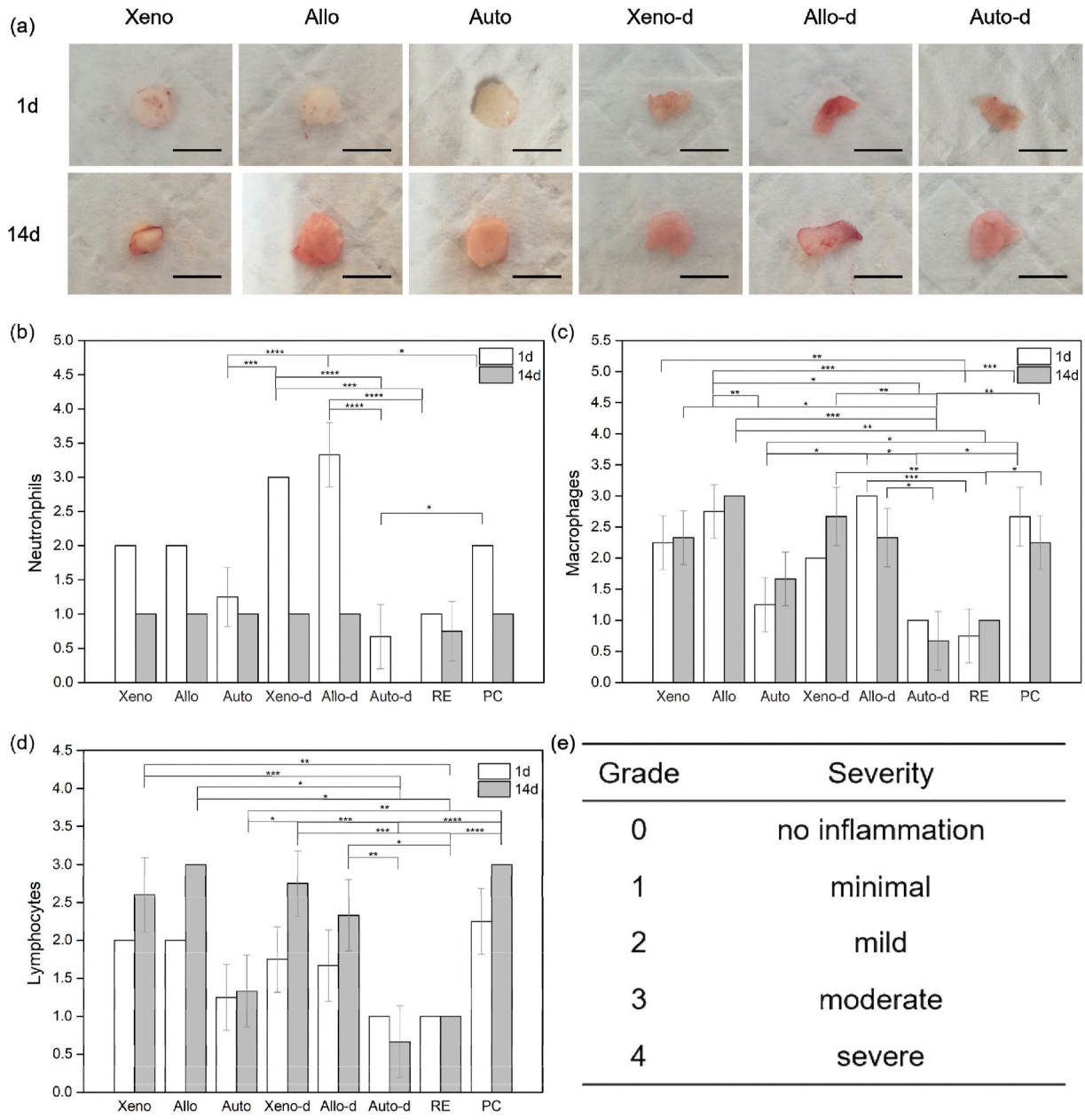

Fig. 6. (a) Photos of samples collected from sacrificed rats. The scale bar is 0.5 cm, and quantitative assessment of immune response according to numbers of inflammatory cells including (b) neutrophils, (c) macrophages, (d) lymphocytes, and (e) the 5-point grading system based on which the samples were evaluated. 0 = no inflammatory cells were seen, 1 = singly dispersed sparse inflammatory cells visible in high power field, 2 = infiltration of inflammatory cells visible in at least one low power field, 3 = abundant inflammatory cells present in every low power field, 4 = samples were badly infiltrated by inflammatory cells observed in low power field (*p < 0.05, **p < 0.01, ***p, <0.001, ****p < 0.0001).

First, the staining results of grafts for day 1 which indicated inflammation in an early immune response phase was shown in Fig. 7a. Xeno graft showed mild infiltration of neutrophils, macrophages and lymphocytes according to pathological analysis. As shown in Fig. 7a, neutrophils (MPO), macrophages (CD68) and T cells (CD3) which were stained in dark brown were found mainly on the surface of Xeno graft. There were mild neutrophils, moderate macrophages and mild lymphocytes present in Allo graft. Neutrophils (MPO) were observed accumulating on the surface of as well as surrounding the deficiency inside Allo graft. CD68 was remarkably stained both on the surface of and inside Allo graft, indicating a much more severe macrophages inflammation compared to Xeno graft. T cells (CD3) were found both on the surface and inside Allo graft. Minimal inflammatory cells were detected in Auto graft. As illustrated in Fig. 7a, only a small number of macrophages (CD68) were observed on the surface of Auto graft with a few T cells (CD3) distributed inside Auto graft. Inflammatory cells were much less in Auto graft than in Xeno and Allo grafts. Abundant neutrophils, mild macrophages and T cells were observed in Xeno-d graft. Neutrophils (MPO) were intensively infiltrated, while macrophages (CD68) distributed dot by dot in Xeno-d graft. Obvious dark brown areas or dots could also be observed in Xeno-d graft stained by CD3. Allo-d graft was graded moderate to severe in neutrophils and macrophages infiltration and mild in lymphocytes infiltration, which was in consistent with the staining results (Fig. 7a). In addition, Allo-d graft displayed much more severe macrophages invasion than Xeno-d graft. In Auto-d graft, inflammatory cells were rarely visible. Grafts collected on day 14 post-implantation were sectioned and stained for evaluation of intermediate phase of acute inflammatory and immune responses

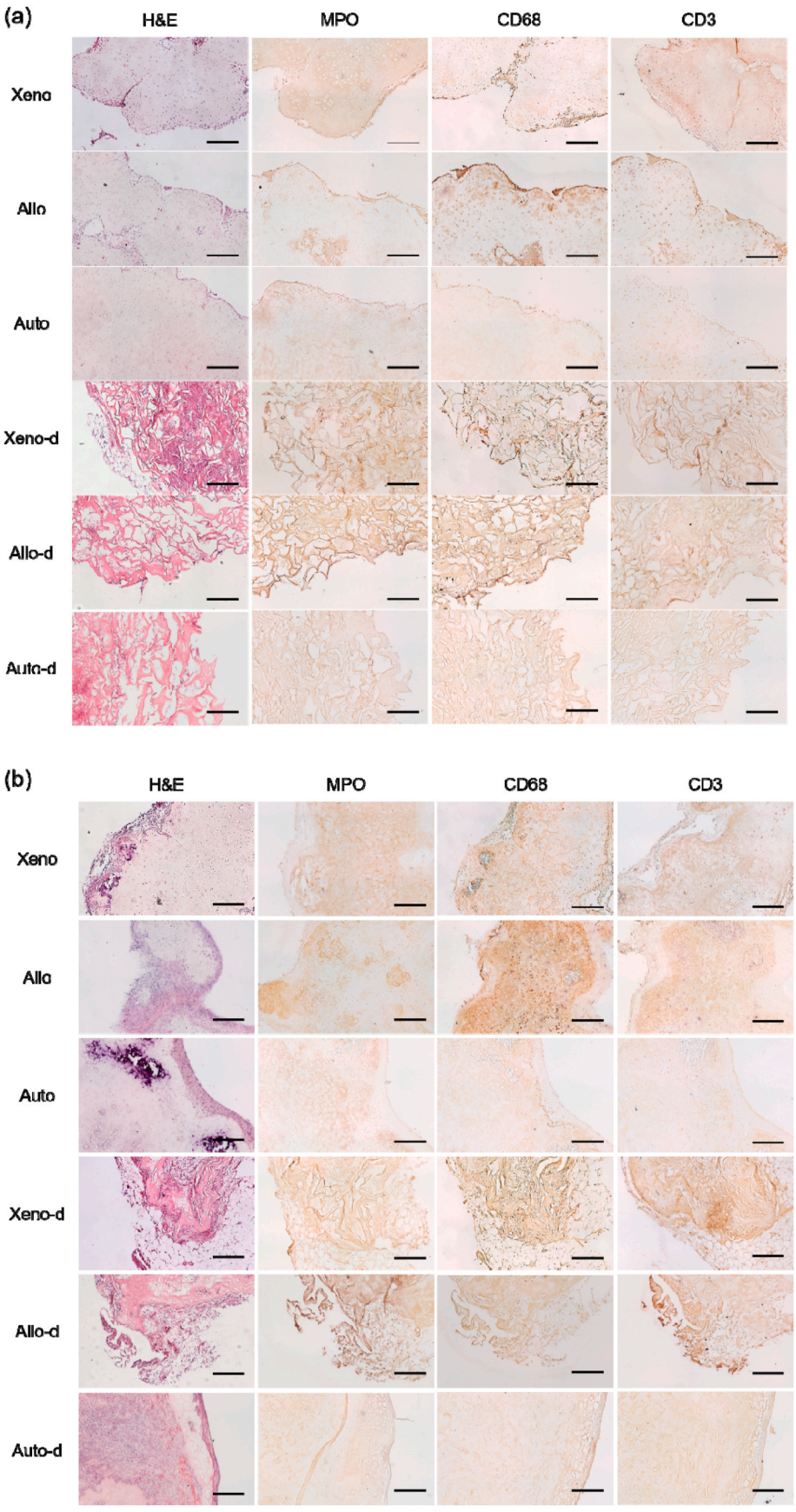

Fig. 7. H&E and IHC staining images for grafts collected on (a) day 1 post-implantation and (b) day 14 post-implantation, scale bar = 250 μm.

(Fig. 7b). Neutrophils infiltration became minimal in all grafts except Auto-d graft which showed nearly no inflammation in neutrophils. MPO was detected inside Xeno and Allo grafts as well as in surrounding tissues of Xeno-d and Allo-d grafts. Macrophages and lymphocytes infiltrations in Xeno graft were between mild and moderate. According to Fig. 7b, obvious CD68 (macrophages) and CD3 (T cells) were observed inside Xeno graft. Moderate macrophages and lymphocytes were recruited on day 14 and found randomly distributed inside Allo graft. There was still mild macrophages infiltration at the boundary between Auto graft and surrounding tissues according to IHC staining image of CD68. T cells

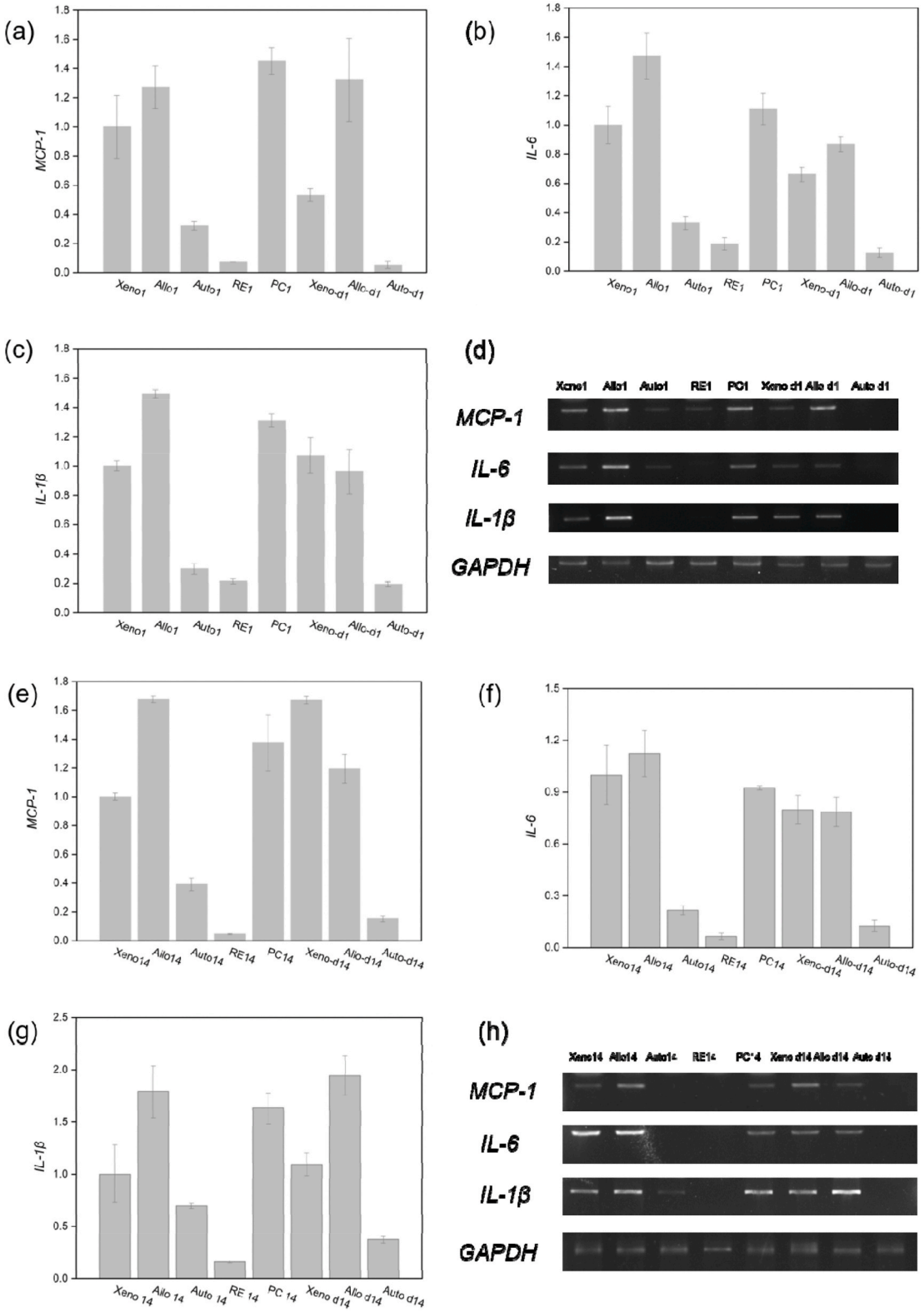

Fig. 8. Gene expression of (a,e) *MCP-1*, (b,f) *IL-6* and (c,g) *IL-1β*, (d,h) gel electrophoresis of *GAPDH*, *MCP-1*, *IL-6* and *IL-1β* for samples collected on day 1 (a ~ d) and day 14 (e ~ h) post-implantation.

were almost invisible in Auto graft, indicating minimal lymphocytes infiltration. Moderate macrophages, which distributed both in graft and its surrounding tissues, and moderate lymphocytes, which mainly distributed in graft especially at the border between graft and surrounding tissues, were observed in Xeno-d graft. The mild to moderate macrophages and lymphocytes recruited were mainly found in the boundary and surrounding tissues of Allo-d grafts. Nearly no inflammatory cells were detected in Auto-d graft.

3.4.3. PCR

After evaluating the immune and inflammatory responses on cell and protein levels and proving grafts with autologous RBC membrane coating were recognized as "self" post implantation, we plan to figure out the performance on a gene level. In the early stage of biomaterial recognition, macrophages released monocyte chemoattractant protein-1 (MCP-1), Interleukin-6 (IL-6) and Interleukin-1β (IL-1β) [58]. MCP-1 regulates migration and infiltration of monocytes or macrophages, recruiting monocytes, memory T cells to the sites of inflammation [59]. IL-6 creates a pro-inflammatory response when signaling in monocytes or macrophages [60]. IL-1β is also a proinflammatory cytokine. Quantitative real-time PCR (qRT-PCR) was carried out on grafts for the evaluation of gene expression encoding inflammation-related cytokines, including *MCP-1*, *IL-1β* and *IL-6*. In order to better compare the inflammatory cytokines mRNA values, we set the gene expression value of Xeno graft as 1 (Fig. 8). The gel electrophoresis results were also shown in Fig. 8 for further confirmation of qRT-PCR results. On day 1 post-implantation, natural porcine cartilage (PC), Allo and Allo-d grafts showed the highest *MCP-1* expression, followed by Xeno graft and then Xeno-d graft. There was slight *MCP-1* expressed in Auto graft and autologous ear cartilage (RE), while *MCP-1* expression was nearly invisible in Auto-d graft. For *IL-6*, Allo graft had the highest expression followed by PC and Xeno, Allo-d grafts, while Xeno-d graft was relatively lower in *IL-6* expression. There was nearly no *IL-6* expression in Auto-d graft and RE. As for *IL-1β*, Allo graft demonstrated the highest expression, followed by PC, Xeno-d, Allo-d and Xeno grafts with obvious *IL-1β* expression. In addition, nearly no *IL-1β* was detected in Auto graft, RE and Auto-d graft. Gene expression results of day 14 post-implantation was shown in Fig. 8b. Allo and Xeno-d grafts showed the highest *MCP-1* expression, followed by PC and Allo-d graft. In addition, Xeno graft also showed obvious expression in *MCP-1*, while Auto, Auto-d grafts and RE were low in *MCP-1* expression. For *IL-6* expression, Xeno and Allo grafts showed the highest value, followed by PC, Xeno-d and Allo-d grafts. *IL-6* expression in Auto, Auto-d grafts and RE was almost invisible. Allo and Allo-d grafts expressed the most *IL-1β*, followed by PC, Xeno-d and Xeno grafts. Slight *IL-1β* expression could be detected in Auto graft, while Auto-d graft and RE showed low value.

4. Discussion

In this study, xenografts were coated with autologous RBC membrane to alleviate immune and inflammatory responses, which is promising in enhancing immunocompatibility in tissue engineering.

The successful extraction of cell membrane was confirmed by ATR-FTIR (Fig. 2a). The RBC membrane vesicles were around 50 nm in diameter according to DLS (Fig. 2b) and AFM (Fig. 2c). Moreover, AFM image confirmed the self-assembly of cell membrane to a globular morphology. The vesicles were negative in zeta potential, which was probably due to the self-assembled cell membrane with hydrophilic phosphoric acid outside and hydrophobic fatty acids inside when suspended in an aqueous solvent. However, cell membrane vesicles were highly unstable with high surface energy and inclined to adhere to solid surface to reduce the free energy, which is the driving force for the successful coating of cell membrane onto grafts. Water contact angle of coverslip increased to 43.4°±0.4° from around 0° after coated with RBC membrane, while that of silicon decreased to 38.1°±1.4° from 59.4°±1.8° after coated with RBC membrane, indicating the feasibility of RBC membrane vesicles to be coated on solid surfaces (Fig. 2d and e). Moreover, it is worth noting that the water contact angle of RBC membrane coating on coverslip was relatively higher than that on Si. When coated on superhydrophilic coverslip surface, RBC adhered to the surface with mainly hydrophilic head attach to the surface and fatty acids tails exposed. Conversely, RBC membrane coated onto Si with fatty acids inside and mainly hydrophilic phosphate head exposed. In addition, as a simulation of LhCG and dLhCG which were derived from chondrocytes extracted from porcine cartilage, natural porcine cartilage was coated with RBC membrane (CM-cartilage) after which water contact angle was measured. CM-cartilage showed a relatively hydrophilic surface with a water contact angle of 37.6 ± 2.0° compared to that of cartilage surface with a water contact angle of 71.3 ± 1.0°, indicating cell membrane vesicles would adhere to cartilage ECM which had a lower surface energy.

RBC membrane, which was dyed with DiO beforehand, was successfully coated onto dLhCG (Fig. 3a) and LhCG (Fig. 3b), respectively according to the fluorescent images. In addition, LhCG was mainly composed of chondrocytes surrounded with glycoproteins and glycosaminoglycan secreted by the cells, while dLhCG consisted of glycoproteins, mainly collagen, and glycosaminoglycan. Cell membrane was a phospholipid with fatty acid tails and a phosphate head. As a result, as is shown in XPS results in Fig. 4 and Table 1, LhCG had a higher phosphorus content than dLhCG. Similarly, there was more phosphorus in CM-LhCG than CM-dLhCG. What's more, phosphorus ratio increased to 2.4% and 3.4% from 0.7% to 2.9% on the surface of dLhCG and LhCG respectively after coated with RBC membrane, implying successful coating of RBC membrane on dLhCG and LhCG grafts. It was reported in our previous study that during decellularization almost all collagen remained while there was a loss of glycosaminoglycan [51]. That is why there was more sulfur detected in LhCG (5.4%) and CM-LhCG (4.8%) compared to dLhCG (3.3%) and CM-dLhCG (2.5%), respectively.

Understanding the stability of the cell membrane coating on dLhCG is also crucial since it takes some time for cells to migrate in the grafts and proliferate after implantation for clinical purpose. For CM-dLhCG, no obvious decrease in P content was detected in 4 weeks. This implied the strong affinity between cell membrane coatings with dLhCG surface and guaranteed the long-term use of CM-dLhCG graft *in vivo* (Fig. 5). This high affinity might also result from the high surface energy of cell membrane vesicles in aqueous environment. The cell membrane vesicles were so unstable that the adherence to graft surface was irreversible. During this time, the cell membrane coating could stay on the dLhCG surface as a disguise. Furthermore, it is worth noting that the coating process did not affect the porous structure of the dLhCG grafts (Fig. 3b and c). For LhCG, CM-DiO was detectable under fluorescent microscope on day 1, day 7, day 14 and day 28, indicating the existence of RBC membrane coatings.

Furthermore, in order to evaluate its immunocompatibility performance *in vivo*, a rat omentum implantation model was applied due to the sensitivity of omentum to foreign bodies. Xenografts with autologous RBC membrane coatings were proved to be superior to xenografts with and without allogeneic RBC membrane coatings in suppressing and alleviating inflammation on cell, protein and gene levels.

After implantation of biomaterials, platelets produced during coagulation secrete cytokines which attract neutrophils from blood stream. In an acute phase of inflammatory response, neutrophils are the first cells to migrate out of the blood stream and head to inflammation site. Then neutrophils release pro-inflammatory cytokines such as IL-6 and IL-1β, promoting the recruitment of the macrophages which are involved in the later phase of inflammatory response and at the same time amplifying neutrophils recruitment. If there is a frustrated phagocytosis, the macrophages will fuse into multinucleated giant cells. Afterwards, those phagocytes present major histocompatibility complex II (MHC II) proteins on their surfaces, which will bind with receptors specifically on T cells and activate them. As the first inflammatory cells to migrate to inflammation site, neutrophils have a short lifespan.

On day 1 post-implantation, macrophages were dominating in the process of inflammation in Xeno and Allo grafts (Fig. 6). Macrophages were recruited into tissues under the trigger of cytokines secreted by neutrophils for phagocytosis of the foreign bodies. For Xeno graft, the inflammatory and immune responses were caused by porcine chondrocytes and antigenic properties of xenogeneic source ECM. Macrophages were observed mainly on the surface with some inside Xeno graft, while neutrophils and T cells were mainly found on and near the surface (Fig. 7a). For Allo graft, macrophages and T cells were found distributed uniformly inside the graft besides accumulating on the surface (Fig. 7a), implying more serious inflammatory and immune responses than Xeno graft. Allo graft presented antigens on allogeneic RBC membrane coatings. Moreover, due to the preference of RBC membrane coating on chondrocytes surface compared to ECM surface and metabolism of chondrocytes, some antigens on LhCG were presented in addition to antigens on allogeneic RBC membrane, which contributed to more severe immune and inflammatory responses in Allo graft than Xeno graft. Xeno-d graft was undergoing an early phase of inflammation with neutrophils dominating (Fig. 6). Neutrophils and macrophages distributed uniformly, while clusters of T cells were found inside Xeno-d graft (Fig. 7a). In Allo-d graft, both neutrophils and macrophages were seriously infiltrated (Fig. 6), indicating the recruitment of macrophages for clearance of foreign bodies and at the same time another initiation of neutrophils infiltration. Therefore, Allo-d graft showed the most severe inflammatory and immune responses on day 1 post-implantation. For positive control, macrophages and lymphocytes were the most prevailing inflammatory cells in PC (Fig. 6), implying a later phase of inflammation had already taken place. In Auto graft, minimal to mild inflammatory cells were detected with relatively more T cells, which indicated slight inflammation occurred. Nearly no inflammation was observed in Auto-d graft and RE. Moreover, Auto-d graft showed significantly reduced neutrophils and macrophages infiltration on day 1 post implantation compared to Xeno-d and Allo-d grafts. Auto graft also showed relatively better performance in neutrophils and macrophages infiltration than Xeno and Allo grafts on day 1 post-surgery.

On day 14 post-implantation, as the first inflammatory cells to migrate in with short lifespan, minimal neutrophils were infiltrated in the intermediate and later phase of acute inflammation and immune responses (Fig. 6b). Moreover, neutrophils were rarely detected in Auto-d graft (Fig. 6b). After 14 days, macrophages and lymphocytes were dominating in inflammatory and immune responses. Allo graft showed the most severe inflammatory cells infiltration on day 14, followed by Xeno graft. The porous structure of dLhCG made it easier for inflammatory cells to migrate in. At the same time the larger specific surface area resulted in a larger contact area with tissues and blood, causing more serious inflammatory and immune responses during an early stage in Allo-d and Xeno-d grafts. However, after two weeks, more antigens on LhCG were exposed and detected, resulting in an increase in macrophages and lymphocytes recruitment which were found mainly distributed inside Xeno and Allo grafts (Fig. 7b). Furthermore, Allo-d graft was going through a later phase of inflammation with lymphocytes dominating and a slight decrease in macrophages infiltration, while Xeno-d graft was undergoing an intermediate phase of inflammation with both macrophages and lymphocytes dominating. As a positive control, PC sample showed heavy infiltration of macrophages and lymphocytes (Fig. 6). There was slight inflammation occurred in Auto graft with mild macrophages detected. Nevertheless, nearly no inflammation was observed in Auto-d graft as well as RE. In addition, Auto-d graft showed significantly reduced macrophages and lymphocytes infiltration compared to Xeno-d and Allo-d grafts, while Auto graft also showed decrease in macrophages and lymphocytes recruitment compared to Xeno and Allo grafts on day 14 post-implantation. Autologous RBC membrane coating on LhCG worked for immune evasion and contributed to better performance of Auto graft in inflammatory and immune responses than Xeno and Allo grafts. However, for Auto graft, due to the preference of RBC membrane coating onto chondrocytes surface and metabolism of chondrocytes, antigens located on LhCG ECM matrix and cells were presented, inducing mild *in vivo* inflammatory and immune responses. dLhCG coated with autologous RBC membrane was recognized as "self" and evaded from immune system attack.

Inflammation is a complicated and highly orchestrated process involving many kinds of inflammatory cells and cytokines. The cytokines are produced and acts as a regulator and stimulator during inflammation process. Therefore, expression of inflammation-related cytokines could reflect severity of inflammatory and immune responses induced. Considering the inflammatory and immune responses have been evaluated on cell and protein levels, evaluation on a gene level, expression of mRNA encoding inflammation-related cytokines, was measured. MCP-1, one of the major chemoattractants for monocytes or macrophages, plays a significant role in inflammation. In addition, it is reported expression of proinflammatory cytokines involving IL-6 and IL-1β was strongly upregulated during inflammation.

Expression of *MCP-1* (Fig. 8) roughly correlated with macrophages infiltration (Fig. 7). It is because MCP-1 played an important role in recruitment of macrophages. On day 1 post-implantation, compared to PC, Allo graft showed more serious inflammatory and immune responses with comparative *MCP-1* expression and higher *IL-6* and *IL-1β* expression; Allo-d graft exhibited slightly lower inflammatory and immune responses with comparative *MCP-1* expression and lower *IL-6* and *IL-1β* expression; Xeno and Xeno-d grafts were lower in inflammation-related gene expression value than PC. Autologous RBC membrane was proved to help suppress or alleviate inflammatory and immune responses on gene level in that dLhCG and LhCG grafts with autologous RBC membrane coating showed an inflammation-related gene expression which was comparative to or slightly higher than autologous rat ear (RE), respectively. 14 days later, dLhCG and LhCG with and without allogeneic RBC coatings as well as PC also showed inflammatory and immune responses with relatively high *MCP-1*, *IL-6* and *IL-1β* expression overall, while Auto, Auto-d grafts and RE with low value in inflammation-related gene expression. Compared to positive control PC, Allo graft showed more serious inflammatory and immune responses with higher inflammation-related gene expression; Allo-d graft exhibited comparative inflammation-relate gene expression; Xeno graft showed a comparative *IL-6* expression and lower *MCP-1*, *IL-1β* expressions; Xeno-d graft had a higher *MCP-1* expression, a comparative *IL-6* expression and a lower *IL-1β* expression. Autologous RBC membrane coating was proved to help suppress or alleviate inflammatory and immune responses on gene level with dLhCG and LhCG grafts with autologous RBC membrane coating a slightly higher inflammation-related gene expression than the negative control RE.

5. Conclusion

This study introduced a novel and facile method to suppress or alleviate immune and inflammatory responses in tissue engineering field by coating autologous RBC membrane on xenografts as a disguise with dLhCG and LhCG as model grafts. First of all, RBC membrane was successfully extracted, coated and quite stable on dLhCG and LhCG for at least 4 weeks. RBC membrane coatings showed no obvious decrease in amount on dLhCG and remained visible on LhCG within 4 weeks. Furthermore, the immune response *in vivo* was evaluated by a rat omentum implantation model. Both LhCG and dLhCG grafts coated with autologous RBC membrane (Auto and Auto-d) showed superior performance in immune evasion on both cell and protein level, especially Auto-d graft with nearly no inflammation detected. It showed enhanced immunocompatibility with less inflammatory cells infiltration in early and intermediate phase of acute host immune responses compared to xenografts with and without allogeneic RBC membrane coatings. Moreover, its enhanced immunocompatibility was also proved on a gene level with low gene expression encoding inflammation-related cytokines including *MCP-1*, *IL-6* and *IL-1β*.

In conclusion, xenografts coated with autologous cell membrane

could be recognized as "self" post implantation. This is proved to be a promising approach for suppression and alleviation of immune and inflammatory responses in tissue engineering field.

CRediT authorship contribution statement

Chao Tao: Methodology, Validation, Formal analysis, Investigation, Data curation, Writing - original draft, Writing - review & editing, Visualization. **Xiaolei Nie:** Investigation. **Wenzhen Zhu:** Investigation, Writing - review & editing. **Jabed Iqbal:** Investigation. **Chenjie Xu:** Resources, Supervision. **Dong-An Wang:** Conceptualization, Methodology, Formal analysis, Resources, Writing - review & editing, Supervision, Project administration, Funding acquisition.

Declaration of competing interest

The authors declare that they have no known competing financial interests or personal relationships that could have appeared to influence the work reported in this paper.

Acknowledgement

We acknowledge the funding support from Shenzhen-Hong Kong Innovation Circle Category D Project (SGDX2019081623180779 to Dong-An Wang), Shenzhen Science and Technology Innovation Commission, China; Grant AcRF Tier 2 Academic Research Fund (MOE2016-T2-1-138 (S) to Dong-An Wang), Ministry of Education (MOE), Singapore; and, Grants from City University of Hong Kong (SGP 9380099, 9240013 and 9678192).

Appendix A. Supplementary data

Supplementary data to this article can be found online at https://doi.org/10.1016/j.biomaterials.2020.120310.

References

[1] S. Franz, S. Rammelt, D. Scharnweber, J.C. Simon, Immune responses to implants-A review of the implications for the design of immunomodulatory biomaterials, Biomaterials 32 (2011) 6692–6709.
[2] Z. Chen, T.D. Palmer, Cellular repair of CNS disorders: an immunological perspective, Hum. Mol. Genet. 17 (2008) 84–92.
[3] A. Oryan, S. Alidadi, A. Moshiri, N. Maffulli, Bone regenerative medicine: classic options, novel strategies, and future directions, J. Orthop. Surg. Res. 9 (2014) 1–27.
[4] W. Ando, K. Tateishi, D.A. Hart, D. Katakai, Y. Tanaka, K. Nakata, J. Hashimoto, H. Fujie, K. Shino, H. Yoshikawa, N. Nakamura, Cartilage repair using an *in vitro* generated scaffold-free tissue-engineered construct derived from porcine synovial mesenchymal stem cells, Biomaterials 28 (2007) 5462–5470.
[5] Q. Yang, J. Peng, Q. Guo, J. Huang, L. Zhang, J. Yao, F. Yang, S. Wang, W. Xu, A. Wang, S. Lu, A cartilage ECM-derived 3-D porous acellular matrix scaffold for in vivo cartilage tissue engineering with PKH26-labeled chondrogenic bone marrow-derived mesenchymal stem cells, Biomaterials 29 (2008) 2378–2387.
[6] H. Lu, T. Hoshiba, N. Kawazoe, I. Koda, M. Song, G. Chen, Cultured cell-derived extracellular matrix scaffolds for tissue engineering, Biomaterials 32 (2011) 9658–9666.
[7] S. Hinderer, S.L. Layland, K. Schenke-Layland, ECM and ECM-like materials-Biomaterials for applications in regenerative medicine and cancer therapy, Adv. Drug Deliv. Rev. 97 (2016) 260–269.
[8] C. Frantz, K.M. Stewart, V.M. Weaver, The extracellular matrix at a glance, J. Cell Sci. 123 (2010) 4195–4200.
[9] A. D'Onofrio, G.D. Cresce, I. Bolgan, P. Magagna, C. Piccin, S. Auriemma, A. Fabbri, Clinical and hemodynamic outcomes after aortic valve replacement with stented and stentless pericardial xenografts: a propensity-matched analysis, J. Heart Valve Dis. 20 (2011) 319–325.
[10] T. Meyer, K. Schwarz, K. Ulrichs, B. Höcht, A new biocompatible material (Lyoplant®) for the therapy of congenital abdominal wall defects: first experimental results in rats, Pediatr. Surg. Int. 22 (2006) 369–374.
[11] P.M. Doran, Cartilage Tissue Engineering-Methods and Protocols, 2015.
[12] H. Lu, T. Hoshiba, N. Kawazoe, G. Chen, Autologous extracellular matrix scaffolds for tissue engineering, Biomaterials 32 (2011) 2489–2499.
[13] R. Cai, T. Nakamoto, N. Kawazoe, G. Chen, Influence of stepwise chondrogenesis-mimicking 3D extracellular matrix on chondrogenic differentiation of mesenchymal stem cells, Biomaterials 52 (2015) 199–207.
[14] E.A. Makris, A.H. Gomoll, K.N. Malizos, J.C. Hu, K.A. Athanasiou, Repair and tissue engineering techniques for articular cartilage, Nat. Rev. Rheumatol. 11 (2015) 21–34.
[15] K.E.M. Benders, P.R. Van Weeren, S.F. Badylak, D.B.F. Saris, W.J.A. Dhert, J. Malda, Extracellular matrix scaffolds for cartilage and bone regeneration, Trends Biotechnol. 31 (2013) 169–176.
[16] Y. Gong, K. Su, T.T. Lau, R. Zhou, D.A. Wang, Microcavitary hydrogel-mediating phase transfer cell culture for cartilage tissue engineering, Tissue Eng. 16 (2010) 3611–3622.
[17] K. Su, T.T. Lau, W. Leong, Y. Gong, D.A. Wang, Creating a living hyaline cartilage graft free from non-cartilaginous constituents: an intermediate role of a biomaterial scaffold, Adv. Funct. Mater. 22 (2012) 972–978.
[18] W. Leong, T.T. Lau, D.A. Wang, A temperature-cured dissolvable gelatin microsphere-based cell carrier for chondrocyte delivery in a hydrogel scaffolding system, Acta Biomater. 9 (2013) 6459–6467.
[19] Y. Peck, P. He, G.S.V.N. Chilla, C.L. Poh, D.A. Wang, A preclinical evaluation of an autologous living hyaline-like cartilaginous graft for articular cartilage repair: a pilot study, Sci. Rep. 5 (2015), 16225.
[20] X. Nie, Y.J. Chuah, W. Zhu, P. He, Y. Peck, D.A. Wang, Decellularized tissue engineered hyaline cartilage graft for articular cartilage repair, Biomaterials 235 (2020), 119821.
[21] X. Nie, J. Yang, Y.J. Chuah, W. Zhu, Y. Peck, P. He, D.A. Wang, Full-scale osteochondral regeneration by sole graft of tissue-engineered hyaline cartilage without co-engraftment of subchondral bone substitute, Adv. Healthc. Mater. 9 (2020), 1901304.
[22] X. Nie, Y.J. Chuah, P. He, D.A. Wang, Engineering multiphasic, integrated graft with biologically developed cartilage-bone interface for osteochondral defect repair, J. Mater. Chem. B 7 (2019) 6515–6525.
[23] A.J. Allman, T.B. McPherson, S.F. Badylak, L.C. Merrill, B. Kallakury, C. Sheehan, R.H. Raeder, D.W. Metzger, Xenogenetic extracellular matrix grafts elicit a TH2-Restricted Immune Response, Transplantation 71 (2001) 1631–1640.
[24] J. Bujia, S. Alsalameh, A. Naumann, E. Wilmes, M. Sittinger, G.R. Burmester, Humoral immune response against minor collagens type IX and XI in patients with cartilage graft resorption after reconstructive surgery, Ann. Rheum. Dis. (1994) 229–234.
[25] E. Dayer, L. Mathai, T.T. Glant, K. Mikecz, A.R. Poole, Cartilage proteoglycan-induced arthritis in BALB/c mice antibodies that recognize human and mouse cartilage proteoglycan and can cause depletion of cartilage proteoglycan with little or no synovitis, Arthritis Rheum. 33 (1990) 1394–1405.
[26] B. Arzi, G.D. Duraine, C.A. Lee, D.J. Huey, D.L. Borjesson, B.G. Murphy, J.C.Y. Hu, N. Baumgarth, K.A. Athanasiou, Cartilage immunoprivilege depends on donor source and lesion location, Acta Biomater. 23 (2015) 72–81.
[27] K.R. Stone, A. Walgenbach, U. Galili, Induced remodeling of porcine tendons to human anterior cruciate ligaments by α-GAL epitope removal and partial cross-linking, Tissue Eng. Part B Rev. 23 (2017) 412–419.
[28] J. Zhou, W. Hu, L. Tang, Non-invasive characterization of immune responses to biomedical implants, Ann. Biomed. Eng. 44 (2016) 693–704.
[29] L. Chung, D.R. Maestas, F. Housseau, J.H. Elisseeff, Key players in the immune response to biomaterial scaffolds for regenerative medicine, Adv. Drug Deliv. Rev. 114 (2017) 184–192.
[30] P.J. VandeVord, H.W. Matthew, S.P. DeSilva, L. Mayton, B. Wu, P.H. Wooley, Evaluation of the biocompatibility of a chitosan scaffold in mice, J. Biomed. Mater. Res. 59 (2002) 585–590.
[31] M.S. Kim, H.H. Ahn, Y.N. Shin, M.H. Cho, G. Khang, H.B. Lee, An *in vivo* study of the host tissue response to subcutaneous implantation of PLGA- and/or porcine small intestinal submucosa-based scaffolds, Biomaterials 28 (2007) 5137–5143.
[32] K. Changi, B. Bosnjak, C. Gonzalez-Obeso, R. Kluger, J.C. Rodríguez-Cabello, O. Hoffmann, M.M. Epstein, Biocompatibility and immunogenicity of elastin-like recombinamer biomaterials in mouse models, J. Biomed. Mater. Res. 106 (2018) 924–934.
[33] K.B. Chien, B.A. Aguado, P.J. Bryce, R.N. Shah, In vivo acute and humoral response to three-dimensional porous soy protein scaffolds, Acta Biomater. 9 (2013) 8983–8990.
[34] J.M. Anderson, A. Rodriguez, D.T. Chang, Foreign body reaction to biomaterials, Semin. Immunol. 20 (2008) 86–100.
[35] A. Dalu, B.S. Blaydes, L.G. Lomax, K.B. Delclos, A comparison of the inflammatory response to a polydimethylsiloxane implant in male and female Balb/c mice, Biomaterials 21 (2000) 1947–1957.
[36] R.A. Manji, W. Lee, D.K.C. Cooper, Xenograft bioprosthetic heart valves : past, present and future, Int. J. Surg. 23 (2015) 280–284.
[37] A. Papalamprou, C.W. Chang, N. Vapniarsky, A. Clark, N. Walker, L.G. Griffiths, Xenogeneic cardiac extracellular matrix scaffolds with or without seeded mesenchymal stem cells exhibit distinct in vivo immunosuppressive and regenerative properties, Acta Biomater. 45 (2016) 155–168.
[38] Y. Suk, J. Jeong, S. Yook, B. Im, J. Seo, S. Woo, J. Park, V.C. Yang, D. Yun, Y. Byun, Biomaterials surface modification of pancreatic islets using heparin-DOPA conjugate and anti-CD154 mAb for the prolonged survival of intrahepatic transplanted islets in a xenograft model, Biomaterials 33 (2012) 295–303.
[39] A.O. Elzoghby, W.M. Samy, N.A. Elgindy, Albumin-based nanoparticles as potential controlled release drug delivery systems, J. Contr. Release 157 (2012) 168–182.
[40] R.H. Fang, Y. Jiang, J.C. Fang, L. Zhang, Cell membrane-derived nanomaterials for biomedical applications, Biomaterials 128 (2017) 69–83.
[41] J.M. Morais, F. Papadimitrakopoulos, D.J. Burgess, Biomaterials/tissue interactions: possible solutions to overcome foreign body response, AAPS J. 12 (2010) 188–196.

[42] S. Naahidi, M. Jafari, F. Edalat, K. Raymond, A. Khademhosseini, P. Chen, Biocompatibility of engineered nanoparticles for drug delivery, J. Contr. Release 166 (2013) 182–194.
[43] D. Tarn, C.E. Ashley, M. Xue, E.C. Carnes, J.I. Zink, C.J. Brinker, Mesoporous silica nanoparticle nanocarriers: biofunctionality and biocompatibility, Acc. Chem. Res. 46 (2013) 792–801.
[44] C.M.J. Hu, L. Zhang, S. Aryal, C. Cheung, R.H. Fang, L. Zhang, Erythrocyte membrane-camouflaged polymeric nanoparticles as a biomimetic delivery platform, Proc. Natl. Acad. Sci. Unit. States Am. 108 (2011) 10980–10985.
[45] A. Parodi, N. Quattrocchi, A.L. Van De Ven, C. Chiappini, M. Evangelopoulos, J. O. Martinez, B.S. Brown, S.Z. Khaled, I.K. Yazdi, M.V. Enzo, L. Isenhart, M. Ferrari, E. Tasciotti, Synthetic nanoparticles functionalized with biomimetic leukocyte membranes possess cell-like functions, Nat. Nanotechnol. 8 (2013) 61–68.
[46] P.Y. Li, Z. Fan, H. Cheng, Cell Membrane bioconjugation and membrane-derived nanomaterials for immunotherapy, Bioconjugate Chem. 29 (2018) 624–634.
[47] P.L. Rodriguez, T. Harada, D.A. Christian, D.A. Pantano, R.K. Tsai, D.E. Discher, Minimal "self" peptides that inhibit phagocytic clearance and enhance delivery of nanoparticles, Science 339 (2013) 971–975.
[48] R.H. Fang, C.M.J. Hu, L. Zhang, Nanoparticles disguised as red blood cells to evade the immune system, Expet Opin. Biol. Ther. 12 (2012) 385–389.
[49] D. Dehaini, X. Wei, R.H. Fang, S. Masson, P. Angsantikul, B.T. Luk, Y. Zhang, M. Ying, Y. Jiang, A.V. Kroll, W. Gao, L. Zhang, Erythrocyte-platelet hybrid membrane coating for enhanced nanoparticle functionalization, Adv. Mater. 29 (2017) 1–8.
[50] C.M.J. Hu, R.H. Fang, B.T. Luk, K.N.H. Chen, C. Carpenter, W. Gao, K. Zhang, L. Zhang, 'Marker-of-self' functionalization of nanoscale particles through a top-down cellular membrane coating approach, Nanoscale 5 (2013) 2664–2668.
[51] Z. Wu, T. Li, W. Gao, T. Xu, B. Jurado-Sánchez, J. Li, W. Gao, Q. He, L. Zhang, J. Wang, Cell-membrane-coated synthetic nanomotors for effective biodetoxification, Adv. Funct. Mater. 25 (2015) 3881–3887.
[52] W. Chen, Q. Zhang, B.T. Luk, R.H. Fang, Y. Liu, W. Gao, L. Zhang, Coating nanofiber scaffolds with beta cell membrane to promote cell proliferation and function, Nanoscale 8 (2016) 10364–10370.
[53] J. Li, A. Celiz, Y. Yang, J.I. Wamala, W. Whyte, B. Seo, N. Vasilyev, J. Vlassak, Z. Suo, D. Mooney, Tough adhesives for diverse wet surfaces, Science 357 (2017) 378–381.
[54] J. Li, M.K.L. Chu, C.R. Gordijo, A.Z. Abbasi, K. Chen, H.A. Adissu, M. Löhn, A. Giacca, O. Plettenburg, X.Y. Wu, Microfabricated microporous membranes reduce the host immune response and prolong the functional lifetime of a closed-loop insulin delivery implant in a type 1 diabetic rat model, Biomaterials 47 (2015) 51–61.
[55] A.V. Kroll, R.H. Fang, Y. Jiang, J. Zhou, X. Wei, C.L. Yu, J. Gao, B.T. Luk, D. Dehaini, W. Gao, L. Zhang, Nanoparticulate delivery of cancer cell membrane elicits multiantigenic antitumor immunity, Adv. Mater. 29 (2017) 1703969.
[56] M. Kovačević, R. Leber, S.D. Kohlwein, W. Goessler, Application of inductively coupled plasma mass spectrometry to phospholipid analysis, J. Anal. At. Spectrom. 19 (2004) 80–84.
[57] D. Pröfrock, A. Prange, Inductively coupled plasma-mass spectrometry (ICP-MS) for quantitative analysis in environmental and life sciences: a review of challenges, solutions, and trends, Appl. Spectrosc. 66 (2012) 843–868.
[58] J.A. Jones, D.T. Chang, H. Meyerson, E. Colton, I.K. Kwon, T. Matsuda, J. M. Anderson, Proteomic analysis and quantification of cytokines and chemokines from biomaterial surface-adherent macrophages and foreign body giant cells 83 (2007) 585–596.
[59] S.L. Deshmane, S. Kremlev, S. Amini, B.E. Sawaya, Monocyte chemoattractant protein-1 (MCP-1): an overview, J. Interferon Cytokine Res. 29 (2009) 313–325.
[60] J. Scheller, A. Chalaris, D. Schmidt-Arras, S. Rose-John, The pro- and anti-inflammatory properties of the cytokine interleukin-6, BBA-Mol. Cell Res. 1813 (2011) 878–888.